42nd AIAA Aerospace Sciences Meeting and Exhibit **AIAA-2004-0472**
5 - 8 Jan, 2004, Reno, Nevada

OPTICAL DISTURBANCES CAUSED BY TRANSONIC SEPARATED BOUNDARY LAYER BEHIND A 20-DEGREE RAMP: PHYSICS AND CONTROL.

Stanislav Gordeyev* and Eric J. Jumper**

Center for Flow Physics and Control
Department of Aerospace and Mechanical Engineering
The Hessert Laboratory
University of Notre Dame
Notre Dame, Indiana

T. Terry Ng† and Alan B. Cain††

Innovative Technology Applications Company
Chesterfield, Missouri

ABSTRACT

In a previous paper [1], we documented the optical disturbance environment created by an attached turbulent boundary layer in high-Mach-number subsonic flow. In the earlier paper, an optical-aberration measurement instrument, the Malley probe, was described and used to collect a high-resolution time series of the optical aberrations for the boundary layer. In the present paper, results using the same instrument will be presented for a high-subsonic, turbulent boundary layer passing a downward 20 degree ramp. In this case, the flow becomes globally separated; the optical aberration environment upon separation starts at the level associated with the turbulent boundary layer but rapidly grows to a much higher level than for the upstream, attached boundary layer. Streamwise and spanwise measurements of Optical Path Difference (OPD) and local convective speeds of the optically-significant structures along the ramp were performed, along with velocity profiles.

The objective of the work was to explore the use of passive devices to reduce the aberration environment created by the separating shear layer. A variety of passive devices placed upstream of the ramp entrance were studied. *Some of these devices had no effect while others resulted in reducing the optical disturbance levels by as much as 50%*.

The paper will describe the experimental set up and each of the devices studied, along with detailed data from the experiments, including the OPD_{rms}, time-series of OPD, and far-field patterns at two wavelengths associated with the baseline data and each of the successful devices. In addition, the paper will discuss the underlying physics of the baseline aberration and the effect of the passive devices. Some description of the theoretical basis for the design of the devices will also be given.

INTRODUCTION

Concepts that involve the projection of relatively-large laser beams from airborne platforms for both civilian and military applications are increasingly coming under consideration. Relevant beam diameters (or apertures, A) range from 0.1 to 0.3 m on the more-common low end to as large as ~ 1.0 m for the AirBorne Laser (ABL) at the upper end. The speed of these envisioned airborne systems range from well subsonic (M ~ 0.1) to moderate subsonic (0.3 < M < 0.5), to transonic (M> 0.8).Concepts are even being formulated for supersonic platforms. All these laser-related concepts depend on the related optical system being able to focus the beam on a distant target.

* Member AIAA, Assistant Research Professor.
**Fellow AIAA, Professor.
† Senior Member AIAA, Vice-President.
†† Associate Fellow AIAA, President

The beam's focusability depends on maintaining a near-perfect wavefront figure across its aperture. Aberrations from this correct figure are usually reported as Optical Path Diference (OPD) from the mean over the aperture, in μm. The effect that these aberration have on the system's performance (i.e., focusability) depends on the laser's wavelength, λ, as a fraction of the beam's wavelength, usually reported in "waves," as OPD/λ. Wavelengths of interest range from the near UV to the near IR (~ 0.35 μm < λ < 1.55 μm), depending on the application.

For the purpose of estimating the system-performance impact, focusability is usually reported as an average Strehl ratio, S_t, which is defined as a time average of the instant-to-instant strehl ratio, given by

$$S_t = \frac{I}{I_0} \qquad (1)$$

where I is the instantaneous in axis intensity and I_o is the diffraction limited on axis intensity. Strehl ratio can be estimated using the large-aperture approximation [3] given the time-averaged OPD_{rms} over the aperture, as

$$\overline{S_t} = \exp\left(-\frac{2\pi\,\overline{OPD_{rms}}}{\lambda}\right)^2 \qquad (2)$$

Using this approximation a tenth of a wave rms aberration reduces the intensity on target by approximately 30%, two tenths of a wave by approximately 80%, and so on. As described above, the OPD_{rms} in Eq. (2) is not only a spatial, but is also a time average; in fact, at any instant in time the Strehl ratio not only depends on the average OPD over the aperture at that instant, but also the aberration scale sizes (or coherence length) in relation to the aperture size. Thus, it is important to treat estimates made using Eq. (2) as only a crude estimate of the systems impact.

The significance of the fact that the laser is projected from an airborne platform is that the beam must pass through the air from the exit puple to the target, any density variations across the beam at any point along its path will produce aberrations on the wavefront figure. Of interest to the present work is only the effect of the turbulent shear flow in the immediate vicinity of the aircraft, and over the aperture; the optical character of this near-vicinity (near-field) aberrating flow is referred to as aero-optics [4].

It is now well known that the aberrating character of the flow depends on whether the flow is attached or separated over the aperture, with the attached case being generally less aberrating than if the flow is allowed is separated over the aperture, all else being equal. Concepts for propagating the beam out of the aircraft include schemes that attempt to only have attached flow (as in some conformal window approaches), as well as always propagating through separated flows (as in fully aft-looking applications and for beam directors embedded in cavities, for example); however, it is generally accepted that the largest field of regard is achieved by propagating from a hemispherical beam director protruding to one degree or another into the slip stream. In this case, unless the flow is made to remain attached over the aft portion of the beam director, look angles greater than approximately 90° back from the oncoming flow cause the beam to propagate through a separated shear layer. Schemes to keep the flow attached for flight Mach numbers greater than about 0.8 can exacerbate the problem by causing shocks to form over the aperture, which can make the problem even worse than allowing the flow to separate. The flow environment is further complicated by the fact that conformal windows are expensive and difficult to maintain, so that most concepts incorporate flat windows. The presence of a flat window on a spherical surface causes a slope discontinuity at the edge of the window. A rule of thumb for estimating the extent of this discontinuity is to assume that the flat window has a diameter no smaller than 1/3 the diameter of the hemisphere. This leads to a slope discontinuity of approximately 27°. It is generally presumed that flow over a hemispherical beam director will remain attached as long as the beam is directed forward ($\leq 90^o$ from the oncoming flow); however, the presence of the discontinuity causes the flow to separate at the corner of the window even at relatively small angles to the oncoming flow, usually reattaching, but at sufficiently high look angles remaining detached over the entire window. It is generally accepted that once the flow separates, the character of the aberration becomes markedly different from when it is attached and the OPD rapidly increases from that in the approaching boundary layer, increasing with distance from separation.

In a previous paper [1], we described the results of studies characterizing the aberrating environment posed by attached, turbulent, subsonic boundary layers up to M = 0.95. In the present study we examined the change in the optical character of the flow as it separates from the wall at the edge of a 20° ramp (expansion) in high-Mach, subsonic flow. The baseline character of the shear layer is documented first and then the change in this character when various passive devices are placed in/on the surface approaching the

ramp. Of importance are the results of how the character of the turbulent boundary are changed once the flow is reattached after separation.

Our study relied primarily on a Malley Probe for characterizing the optically aberrating flow field; the theory, operation and implementation of the instrument was described in detail in our previous, boundary-layer paper [1]. In that which follows, we will describe the experimental set up, followed by the characterization of the baseline separated flow. Following this, each of the devices studied will be described along with their effect on the optical character of the flow. Finally, some conclusions will be drawn that follow from the results. In particular, these conclusions will contain a discussion of the aberrating character contained in a reattached boundary layer, even when the separated region is relatively short.

EXPERIMENTAL SET-UP

Our goal has been to reproduce realistic flight conditions as close as possible in order to investigate practically important boundary layer cases. With this in mind, we focused primarily on Mach numbers between 0.6 and 0.95. Further, we intentionally grew canonical turbulent boundary layers that were of realistic thickness so that our Reynolds numbers based on boundary-layer thickness were in the range that could be expected for beam-directors on contemplated laser fighters. Because the tests were ran in an indraft facility, this also gave the benefit of a range of pressure altitudes that aided in our scaling-rule development and guaranteed that our studies simulated flight conditions above sea level. With this in mind, the experiments reported on here were performed in a transonic indraft wind tunnel located in the Hessert Laboratory at the University of Notre Dame. The tunnel consisted of a 150:1 contraction inlet, a series of specially-constructed test sections, and a diffuser (see Figure 1a). The diffuser joins to a large gated plenum. The plenum is pumped to low pressure by up to three Allis Chalmer 3,310 CFM vacuum pumps. By selecting the proper valve settings, the tunnel can be pumped by one, two or three pumps; the present experiments used either one or two pumps depending on the specific Mach number.

All test sections started with a first component whose cross section was 9.9-cm x 10.1-cm, matching the dimensions of the tunnel inlet. The lower wall of this component (which was the side of the tunnel whose boundary layer and subsequent shear layers were investigated) was covered with medium grain sandpaper along its 50 cm length to facilitate the onset and initial growth of a turbulent boundary layer. After this component, specific test section configurations were formed by adding components to increase or shorten the test section's length, thereby effectively adjusting the boundary layer's thickness. Following the sandpaper, the boundary layer was allowed to grow naturally over varying tunnel lengths from 60 to 110 cm, depending on the test section's configuration.

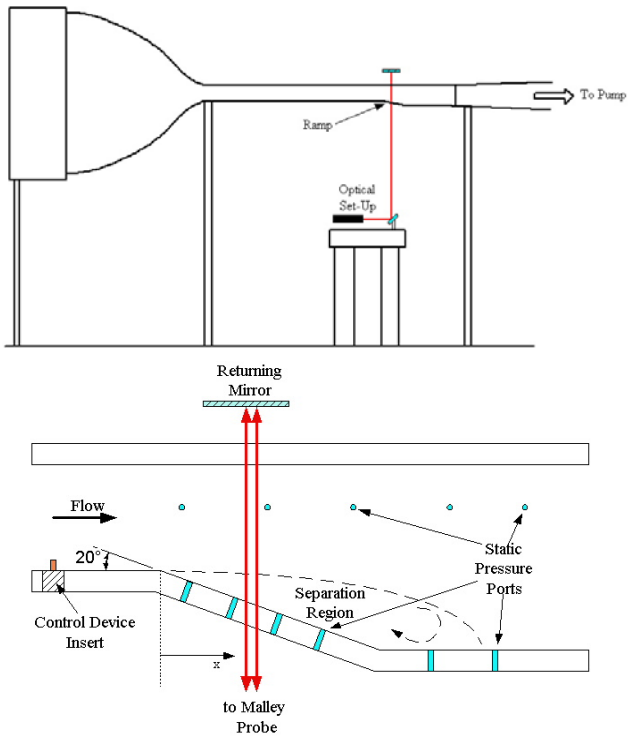

Figure 1. (a) Schematic of the tunnel set-up and (b) the 20-degree ramp instrumentation.

For the separated, turbulent-boundary-layer and shear layer experiments, additional components were constructed. The basic module for these was a 69 cm section matching the width of the boundary-layer components (9.9 cm), but with an abrupt increase in height to 14.4 cm configured so that it formed a 4.5 cm step on the lower wall of the section. In order to form mildly-separated flow regions, this "step" was softened with the experimental-configuration ramp with an angle of 20 degrees. Figure 1b presents a schematic of the 20-degree ramp test section showing locations of the pressure static ports and a passive control device, used to modify the separated boundary layer. It should be noted that this is roughly the discontinuity angle that a hemispherical beam director would see at the leading

edge of a flat window when the beam director is slued to 90° azimuth at all elevations. The entire test sections, ramp and walls were made of Plexiglas so that both flow smoke visualization and Malley probe measurements could be made along the entire ramp and remaining tunnel wall.

Although a number of Mach number cases and inflow boundary layer thicknesses were examined, the results shown here for the baseline cases were for Mach numbers of approximately 0.85, and two inflow boundary-layer displacement thickness before the ramp entrance of approximately 3.4 and 4.4 mm.

Malley Probe Measurements. Throughout the history of aero-optics research there have been a number of proposed methods of making appropriate optical measurements; however, as has become abundantly clear in the last decade, the only appropriate measurement for assessing optical degradation due to aero-optic flow environments is time-resolved, correlated time series of *actual or fully-characterized wavefronts*. This is because single, uncorrelated wavefronts either by interferometers or wavefront sensors first require their collection in large numbers to draw any statistical meaning from them, but in a real sense are unable to provide spatial and temporal frequencies. Similarly, hot-wire-based measurements that infer optical degradation by the use of linking equations suffer from similar ambiguity over spatial and temporal frequencies as well as having now been called into some question concerning the amplitude of the disturbances (although qualitative scaling laws have, in some cases, been shown to be justified). Being able to collect time series of time-resolved, correlated wavefronts in the usual sense of collecting these measurements using two-dimensional Hartmann sensors, places extraordinary burdens on instrument-tation. Studies performed over the last decade have shown that for high-Mach flows wavefronts should be collected at up to 30 kHz to capture the character of the shear and boundary layer aero-optic phenomenon of interest. While these bandwidths are within the present abilities of fast CCD arrays that might be employed for a fast Hartmann sensor, the number of consecutive frames per series is limited. On the other hand, instrumentation already developed and in continuing development at Notre Dame, particularly the Small-Aperture Beam Technique (SABT) sensor is routinely used to collected long time series of actual wavefront cuts in the streamwise direction at up to 150 kHz [2,3]. This instrument, in fact, is responsible for the quantum breakthroughs over the last decade in the understanding of high-Mach aero-optics [4]. For the present study an even more efficient instrument that *fully characterizes the wavefronts* and their dynamics, as described in [1,5] a Malley probe, was used.

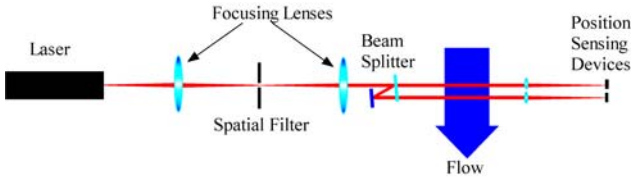

Figure 2. Schematic of the Malley probe.

An advanced version of a Malley probe [1] was refined and used to perform the optical measurements in the present study. A Malley Probe is an optical instrument that can make direct, accurate measurements of actual dynamically-distorting wavefronts at a localized region of an aperture as OPD($x\pm\Delta,t$), and these data used to extend this accurate measurement over a larger region of the aperture [5,1]. By moving the instrument, an entire, large aperture can be fully characterized optically, both spatially and temporally, over the entire aperture. This characterization includes not only the measurement of OPD_{rms}, but also the spatial and temporal frequencies of the aberrations as well as actual time histories of the dynamic figure of the wavefront. *Having these times series of wavefront figures allows for the construction of far-field intensity patterns so that system-performance degradations/improve-ements due to the aero-optic environment with and without control may be inferred.*

The instrument itself is a further development by Notre Dame of an instrument described in a paper by Malley et. al. [5]. In that paper, a working instrument was developed and applied to an aero-optical flow and shown to be consistent with OPD_{rms} estimates made using a limited number of interferograms for the same flow field. The Notre Dame, Malley-derivative sensor is an advancement over the one described in Malley et. al. [5], with the inclusion of a second, closely-space probe beam and the development of robust methods of extracting the information needed to give extremely accurate characterizations of the wavefront [2]. The instrument consists of two closely spaced beams (~2 - 8 mm apart and aligned, front beam to aft beam, in the streamwise direction); the second beam is used to extract phase-velocity data contained on the beam-deflection angles by cross correlating them and obtaining the time delay for maximum correlation [1]. Knowing the displacement between the beams and this delay time, the phase velocity can be computed. As

described in Hugo and Jumper [2], the deflection angle of the probe beam is the spatial derivative of a wavefront for a larger-aperture, otherwise planar wavefront that would be present if that wavefront were aberrated by the same flow. The group velocity is needed to unfold the OPD using the fact that the aberrations "convect" with convecting fluid structures; this fact was first discussed by Malley et. al. [5].

A general schematic of the Malley probe is shown in Figure 2. The beam separation was set at 5 mm throughout all measurements reported here. After traversing the test section and passing through the applicable lens, the beams were directed to two positions sensing devices, PSD; the signals from the PSD's were used to record the displacement of the beams as a function of time, from which the wavefront slope was extracted. Although the device is capable of measuring wavefronts at 150 kHz, based on preliminary measurements of the temporal frequencies present in the dynamic aberrations, the sampling rate was set to f_{samp} = 50 kHz. The total number of samples collected per channel in these tests was 16,384, giving a total sampling time of 0.328 sec. In every case many of these 0.328 sec data records were collected for each test condition Two test section lengths, *L*=110 and 160 cm, were used for the data presented here. These sections for M=0.85 provide boundary layer displacement thicknesses of δ^*=3.4 mm and 4.4 mm before the ramp entrance, respectively.

Flow Visualization: On- and off-surface flow visualizations were used to determine the baseline flow characteristics. Flow patterns over (i.e., not taking the on-surface visualization into account) the ramp is shown schematically in Figure 1b. The 20-degree ramp flow visualization was unambiguous and showed that it was separated over the entire ramp but reattached on the lower wall of the test section at approximately an additional ramp length.

Baseline Flow Measurements: Because both the tunnel walls and the ramp were made of Plexiglas, the Malley probe was used to make optical measurements for propagation through the shear and reattached boundary layers at different streamwise positions along and beyond the ramp. As described before, the Malley probe not only measures OPD(t), but also the aberrating-structures' convection velocities. The results for the aberrations' convective velocities and its OPD_{rms} for the ramp are shown in Figure 3. This case is called the baseline case, since effects of control devices will be later compared against it.

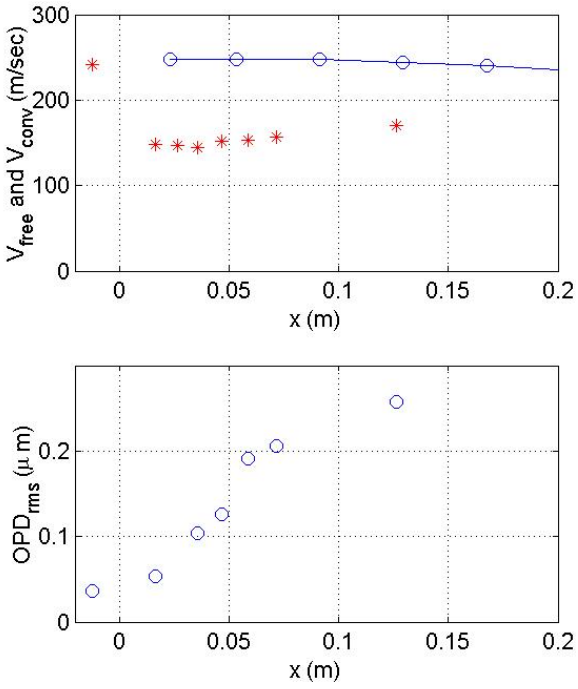

Figure 3. Streamwise variation of OPD over the ramp: Baseline case.

It should be noted that Figure 3 shows data for a single point where the boundary layer is fully attached just upstream of the ramp onset at *x* = -0.015 m. Notice that the velocity of the aberration is close to the freestream velocity at that point, consistent with the findings in [1]; after the onset of the ramp the aberrations are clearly moving at the expected convection velocity in a free shear layer, which is approximately 0.6 of the freestream velocity. In the lower plot of Figure 3, the optical aberrations in the attached boundary layer are consistent with [1] and then begin to grow. The growth does not stop at the mid-ramp position and continues to grow after the ramp ends at x=0.1 m, reaching a final OPD_{rms} of approximately 0.27 microns (a growth of more than 5 times that of the attached turbulent boundary layer) at the last location measured. This too is consistent with what has been reported for a free shear layer, and it represents an extremely poor propagation environment for a laser with a 1 μm wavelength. Although not shown in these data, later data presented in the next section show that the growth continues until the shear layer reattaches; however, once reattached the degraded optical propagation environment persists, decaying slowly over extended lengths.

Figure 4. Pin configurations and, in the closest configuration, the cavity configuration.

Passive Devices Measurements

As mentioned in the previous section, the stronger adverse pressure gradient over 20-degree ramp caused the incoming flow to fully separate at the ramp edge. And, as also mentioned above, flow visualization showed that the flow remained separated over the entire ramp, reattaching at approximately 0.2 m downstream from the onset of the ramp, i.e., approximately 0.1 m past the end of the ramp. The separated flow over the ramp formed a strong shear layer with characteristics similar to those formed using classical splitter plates, and the rapid growth in the optical aberrations in the baseline flow, described before, is consistent with those expected for this type of layer. Referring back to the baseline data for the 20-degree ramp, it can be seen in Figure 2 that the convective speeds are roughly 0.6 of the local freestream speed, which is a typical value for a shear layer. The OPD_{rms} linear growth in Figure 2 reaches levels of 0.27 μm by the end of the ramp. In the 20-degree study our approach was to attempt to suppress or delay the formation of coherent structures in the shear layer.

As mentioned in the *Introduction*, computational studies by one of the authors, as well as experimental studies by others, suggested that one way to suppress the formation of the coherent vortical structures responsible for the aberrations seen in the baseline cases would be to introduce high-frequency disturbances into the incoming boundary layer. One way this can be accomplished is by inserting one or multiple rows of small vertical cylinders into the boundary layer upstream of the separation point. Cylinders shed vortices, which in turn interact with the boundary layer and create small-scale 3-dimensional disturbances. Another way to create disturbances is to place cavities in the wall below the incoming boundary layer. Both of these approaches for introducing high-frequency disturbances were investigated.

A variety of high-frequency-generating devises, shown in Figure 4, were constructed and placed into the lower wall of the test section 5 cm upstream of the ramp edge and tested under a variety of flow conditions to see if they could improve the optical-propagation environment over that present in the baseline flow. The following devices were investigated:

1. Spanwise rake of cylindrical pins normal to the surface, 1 mm diameter, 2.5 mm apart, 6 mm high and 5 cm upstream from the ramp.
2. Spanwise rake of cylindrical pins normal to the surface, 3 mm diameter, 6 mm apart, 7 mm high and 5 cm upstream from the ramp.
3. Spanwise rake of cylindrical pins normal to the surface, 5 mm diameter, 10 mm apart, 10 mm high and 5 cm upstream from the ramp.
4. Spanwise rake of cylindrical pins normal to the surface, 1 mm diameter, 6 mm apart, 6 mm high and 5 cm upstream from the ramp.
5. Spanwise series of cavities recessed into the surface, 5mm depth, 17 mm length, 4 mm width and 5 cm upstream from the ramp.
6. Combination of spanwise series of cylindrical pins normal to the surface: 1 mm diameter, 2.5 mm apart, 6 mm high and 2 cm upstream from the ramp; and 3 mm diameter, 6 mm apart, 7 mm high and 5 cm upstream from the ramp.
7. Combination of spanwise series of cylindrical pins normal to the surface: 3 mm diameter, 6 mm apart, 7 mm high and 2 cm upstream from the ramp; and 1 mm diameter, 2.5 mm apart, 6 mm high and 5 cm upstream from the ramp.

Vortex-shedding pins. The rational for choosing the pin rakes was that when the pins protrude into the boundary layer they produce von Karman streets of radial vortices that tilt into the shear layer due to the strained velocity field. It is known that over some portion of the boundary layer thickness the streets are approximately periodic in ***space and time*** and undergo substantial vortex stretching producing fine scale vorticity. Results for several pin configurations and the baseline, for the thicker boundary layer, δ^*=4.4 mm, are shown in Figure 5.

First, it should be noted in Figure 5 that all of the pin configurations produced a decrease in the aberration

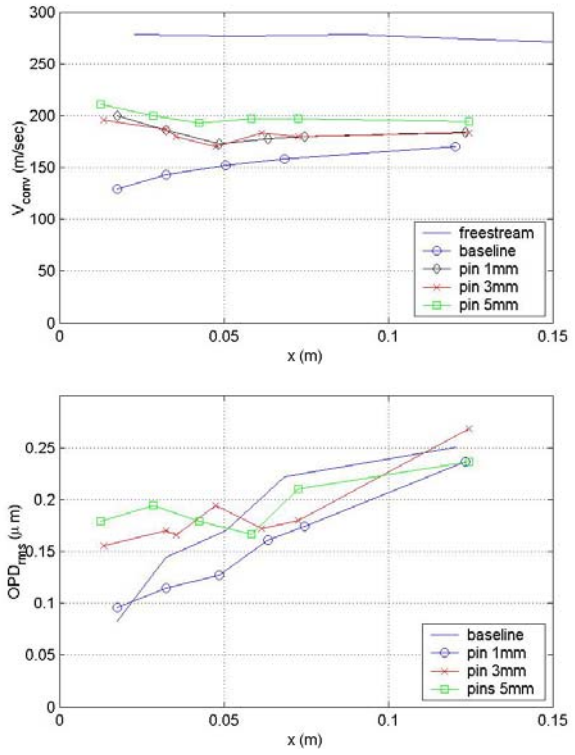

Figure 5. Effect of different pins on optically aberrating structures for the thicker boundary layer δ^*=4.4 mm.

environment over some portion of the length of the test section! The most-beneficial control of the configurations tested can be seen to be provided by the 1-mm pins, in this case in the configuration shown in Figure 4, just behind the cavity configuration. As shown in Figure 5, the 3 and 5-mm pins caused an initial increase in the optical aberration relative to the baseline. The streamwise rates of increase in the OPD_{rms} for the 3 and 5-mm pins were, however, slower than the baseline case, and the optical aberration became smaller than the baseline farther downstream. In comparison to the larger pins, the 1-mm pins produced virtually no initial increase in the OPD_{rms} while maintaining a similarly low streamwise rate of increase. This resulted in a reduction in the OPD_{rms} of up to 30% over all the downstream locations measured. It is interesting to note in Figure 5 that in every case, the pins caused an increase in the convective velocity over that of the baseline due to an enhanced mixing with the high speed free-stream portion of the flow, most noticeably at the onset of the ramp.

Results for a thinner boundary layer, with δ^*=3.4 mm, are presented in Figure 6. As has been pointed out previously, it is important to note in Figure 6 that the ramp ends at 0.1 m, with the flow reattaching at approximately 0.2 m. As mentioned in the baseline section above, the OPD_{rms} continues to grow until reattachment and then *only slowly* decays. It is clear from the data in Figure 6 that the pin rakes provide an even greater reduction in OPD_{rms} over that seen for the thicker boundary layer case of Figure 5. As in the case of thicker boundary layer, 1 mm pins perform the best, but now they lower OPD_{rms} over the entire ramp by a factor of 2. Other pin configurations also reduce optical aberrations over most of the ramp, although to a lesser degree.

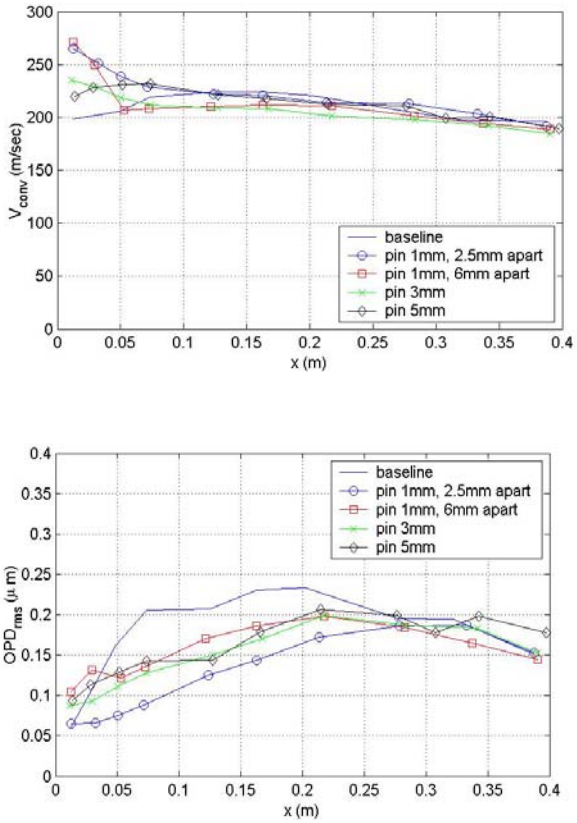

Figure 6. Effect of different pins on optically aberrating structures for the thinner boundary layer δ^*=3.4 mm.

Figure 6 also shows optical characteristics of the flow behind the ramp (beyond 0.1 m). It can be seen in the baseline case that the growth in OPD_{rms} appears to plateau at approximately the end, but continues to grow until 0.2 m where the flow visualization indicated that the flow reattaches. After reattachment the OPD_{rms} begins a slow decay. All of the pin configurations tested improve the optical propagation characteristics over the ramp, except, in the case of the larger pins, at the very onset of the ramp. It should be noted because of its

design-space implications that there is a clear difference in effectiveness in placing the 1 mm pins 2.5 mm apart vs. 6 mm apart, the closer spacing being more effective. In fact, for approximately 5 cm, the closer-spaced 1 mm pins keep the propagation characteristic at almost the level of the feeding attached turbulent boundary layer. In all cases, the pins continue their improved propagation environment up to and even beyond the baseline's reattachment point. Although because of time limitations flow visualization done for any but the baseline cases, if one infers from the baseline case that the reattachment point corresponds to a point where OPD_{rms} reaches a maximum value, one might conclude from Figure 6 that pins delay reattachment by as much as 0.3 m for the closely-spaced 1 mm pin configuration. Figure 6 also shows the convective speeds for the different configurations. The effect of the pins on the convective velocity is similar to that for the thicker boundary layer. Thus, the pin configurations placed into the boundary layer ahead of the ramp clearly change the flow over the ramp resulting in a reduction in optical distortions caused by flow structures.

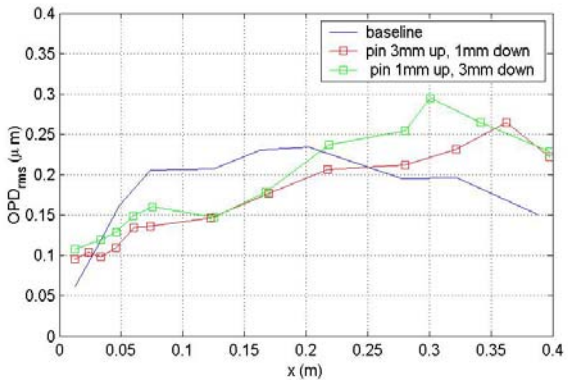

Figure 7. Effect of different pins' combinations on optically aberrating structures for the thinner boundary layer δ^*=3.4 mm.

An important conclusion can be drawn from Figure 6, that was mentioned previously in the *Baseline Section* but is worth stating again; even after reattachment, the reattached boundary layer still carries a significant amount of optical distortions created in the separated shear layer and, as a result, OPD_{rms} levels do not go down to pre-ramp levels immediately after the reattachment. Rather there is a slow, gradual process of decay that takes place. Even after 20 cm of reattachment the aberration environment is more than 3 times worse than that for the attached boundary layer before the ramp. Therefore, memory effects imprinted in the boundary layer after reattaching itself are significant and should be addressed properly in future work.

Combinations of pin rakes were also tested; two of these combination configurations will be described. The first configuration consisted of a 1mm pin rake placed 5 cm upstream of the ramp edge with a 3 mm pin rake behind the 1 mm rake, 2 cm upstream of the ramp edge. The second configuration was similar to the first but with the rakes switched. Results for these configurations are plotted in Figure 7.

Referring back to Figure 6, the combination rakes essentially perform as a single rake and reduce OPD_{rms} distortion by approximately 30% over the ramp span. While there are subtle difference in the character of the improved optical environment that may be of interest in attempting to optimize configuration in follow on work, these combinations show no particular improvement over the single row rakes for distances out to the baseline reattachment point. One clear difference, however, occurs after that point; the combination rakes delayed the reattachment point until 0.3 to 0.35 m, allowing the aberrations to continue to grow, eventually beyond that of the baseline case.

Resonance cavities. The resonance cavity concept is based on producing high-frequency disturbances by inducing acoustic resonance in rectangular cavities. In operation a series of cavities, tuned to operate at the desired frequency for the flow Mach number, are placed upstream of the separation point. The high-frequency disturbances produced are then convected downstream to effect control over the development of the shear layer. Earlier simulations, run by one of the authors and reported in [6], were performed to estimate the optimal frequencies for quieting the supersonic cavity flow. The simulations themselves actually applied to a wake flow but it was hoped that the results could be extended to any inflectionally dominated free shear flow where the inviscid instability is dominant. The assumed scaling was based on the neutral frequency of any given flow.

Cain et al [6] suggested that the most effective forcing frequency for the high frequency effect is approximately 2-3 times the neutral frequency of a wake flow. The same criteria were applied to the present application. The dominant resonances of the cavities were estimated using the *Graphical User Interface* for cavity resonance prediction developed in Cain et al. 1997 [7]. It is important to realize that there

is only a narrow window of viability for the cavity excitation scheme. The reason for this is that the boundary layer shields the cavity from the freestream and as the cavity becomes short compared to the boundary layer thickness the cavity resonance becomes vanishingly small, on the other hand if the cavity is too long the frequencies produced are too low in frequency. For this reason, the cavity configuration designed and constructed for this test series, as shown in Figure 4, was designed to be effective for the thicker, δ^*=4.4 mm, boundary layer, but tested for both the thicker and thinner boundary layer to see if the design criteria could be shown to correctly predict that it would be effective only in the thicker-boundary-layer case.

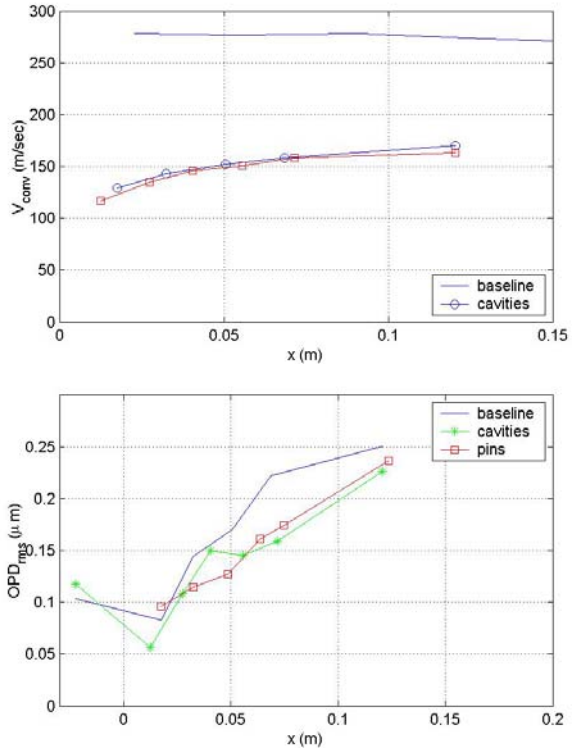

Figure 8. Effect of 1mm pins and cavities on optically aberrating structures for the thicker boundary layer δ^*=4.4 mm.

Results for the cavity configuration tested for the thicker boundary layer, δ^*=4.4 mm, along with that for the baseline and the most-effective pin rake are shown in Figure 8. As shown in Figure 8 the cavities do not produce the a small initial increase in the OPD_{rms} caused by the pins, but rather track the baseline with a slight improvement for approximately 4 cm. This results in a slightly reduced amount of improvement in the propagation environment from that of the pins out to and beyond 4 cm; however after 6 cm the cavity configuration matches and is even a slight improvement over the effectiveness of the pins. This change over from tracking the baseline to matching the pins performance is due to a noticeable plateauing in the optical environment at 4 cm that persists for 2 cm, where the streamwise rate of increase in the OPD_{rms} of the cavities is seen to approximate that of the pins, which is slower than the baseline case; the optical aberrations are smaller than the baseline from then on. The result is a reduction in the OPD_{rms} of up to 30%. Figure 8 shows that, unlike the pins (see Figure 5) where there is a noticeable change in the convection velocity at the beginning of the ramp, the cavities caused virtual no change in the convective velocity compared to the baseline in this region, since they don't increase a turbulent mixing with the free-stream flow, but rather impose periodic disturbances on the boundary layer; coincidentally, referring back to Figure 8, in this region the optical environment tracks that of the baseline, whereas the pins show an improvement in this region over that of the baseline.

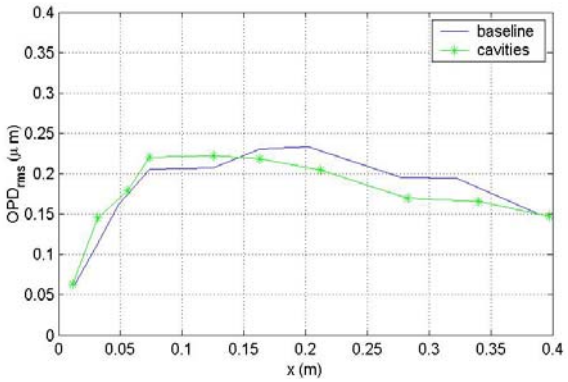

Figure 9. Effect of cavities configuration on optically aberrating structures for the thinner boundary layer δ^*=3.4 mm

The cavity configuration's performance with the thinner boundary layer is shown in Figure 9. As mentioned earlier, this result, which shows essentially no improvement in the propagation environment, is a *positive result*! The fact that the configuration was effective in improving the propagation environment for the thicker boundary layer, δ^* = 4.4 mm, test series, but ineffective for the thinner boundary layer, δ^* = 3.4 mm, test series validates the design rules developed in the earlier reference work. Thus bodes well for future efforts that will be directed toward producing optimization rules and design tools.

CONCLUSIONS

Optical aberrations caused by a separated boundary layer over the 20-degree ramp for high subsonic Mach numbers M=0.85 for two different incoming boundary layer displacement thicknesses of 3.4 and 4.4 mm were measured using the Malley probe set-up. It was established that after the boundary layer is separated it quickly creates higher levels of optical distortions versus ones for the fully attached boundary layer. These high levels (2-3 times higher than the ones in the attached boundary layer) persist throughout the separated region and remain to be high for significant distances downstream even the boundary layer reattaches itself further downstream.

Different passive devices, namely, vertical pin rakes and cavities configurations were placed just upstream of the ramp entrance in order to modify the separated boundary layer and subsequently it's optical characteristics. It was found that almost all of them do decrease optical distortions, although by different degrees, by either introducing small spanwise shedding vortices in the case in pins configurations or imposing high frequencies fluctuations on the incoming boundary layer in the case of the cavity configuration. The small 1mm pin configurations were found to perform the best in all tested cases and decrease the optical aberrations by 30 – 50 %. All pin configurations increase the convective speeds of the structures in the separated boundary layer by enhancing the mixing with the high-speed free-stream flow. Cavities' performance was found to be sensitive to the incoming boundary layer thickness. When properly tuned for a given incoming boundary layer, cavities perform as good as the 1 mm pin rake configuration and virtually have no effect on the flow in other cases.

ACKNOWLEDGEMENT

This work was supported through an AFOSR STTR contract, contract number F49620-02-C-0051. This effort was conducted under the program management of Dr. Thomas Beutner.

References

[1] S. Gordeyev, E. Jumper, T. Ng and A. Cain, "Aero-Optical Characteristics of Compressible, Sub-sonic Turbulent Boundary Layers", AIAA Paper 2003-3606, Orlando, FL, June 2003.

[2] Hugo, R.J., and Jumper, E.J., "Quantification of Aero-Optical Phase Distortion Using the Small-Aperture Beam Technique", *AIAA Journal*, **33**(11), 1995, pp. 2151-2157]

[3] Mahajan, V.N., "Strehl Ratio for Aberration in Terms of Their Aberration Variance", *J. Opt. Soc. Am*., **73**, 1983, pp. 860-861.

[4] Jumper, E.J., and E.J. Fitzgerald, "Recent Advances in Aero-Optics", *Progress in Aerospace Sciences*, **37**, 2001, pp.299-339.

[5] Malley, M., Sutton, G.W., and Kincheloe, N., "Beam-Jitter Measurements for Turbulent Aero-Optical Path Differences", *Applied Optics*, **31**, 1992, pp. 4440-4443.

[6] Cain, A.B. and Rogers, M.M., "Characterization of High-Frequency Excitation of a Wake by Simulation", Submitted for presentation at the Aerospace Sciences Meeting, Reno, NV, Jan., 2003.

[7] Cain, A., Bower, W., McCotter, F. and Romer, W., "Modeling and Prediction of Weapons Bay Acoustic Amplitude and Frequency", Final Technical Report submitted to VEDA Inc., 1996.